



DØnote 5892-CONF

Search for a fourth generation t' quark that decays to W boson + jet

The DØ Collaboration

URL <http://www-d0.fnal.gov>

(Dated: July 14, 2010)

We present a search for pair-production of a fourth generation t' quark with its antiparticle, followed by their decays to Wq , based on 4.3 fb^{-1} of proton-antiproton collisions at $\sqrt{s} = 1.96 \text{ TeV}$ collected by the DØ Collaboration at the Fermilab Tevatron. We set upper limits on the $t'\bar{t}'$ production cross section which allows us to exclude a sequential t' quark that decays exclusively to Wq with a mass below 296 GeV at 95% CL.

I. INTRODUCTION

We present a search for pair-production of a new massive quark (t') in the lepton+jets final state using 4.3 fb^{-1} in $p\bar{p}$ collisions at $\sqrt{s} = 1.96 \text{ TeV}$. The data were acquired by the D0 Collaboration between June 2006 and September 2009 at the Fermilab Tevatron collider. We use as a bench mark pair production of a fourth generation up-type quark that decays exclusively to Wq .

Measurements of the partial width of the Z boson to invisible final states at LEP exclude the existence of a fourth neutrino flavor with mass less than half the Z boson mass [1]. However, this does not exclude a sequential fourth generation of fermions. The χ^2 of the global electroweak fit does not get worse when a fourth generation of fermions is included with a neutral lepton with a mass that is a few GeV above half the mass of the Z boson [2]. The up-type quark of this fourth generation, t' , can either decay to its down-type partner, b' , or to a standard model down-type quark q plus a W boson. For $m(t') - m(b') < m(W)$ and moderate mixing between t' and q , the $t' \rightarrow Wq$ decay mode will dominate [3].

One can easily eliminate all restrictions on fourth generation fermions by hypothesizing that the new massive quark is vectorlike, i.e., that it is not part of a weak isospin doublet. Such a particle appears, for example, in little Higgs models that require the existence of a vectorlike quark T as a partner, of the top quark. The T can be pair-produced in $p\bar{p}$ collisions if its mass is not too high and the decay $T \rightarrow Wq$ is expected to have a branching fraction of about 50% [4].

Here we report on a search for a fourth generation t' quark that is produced in proton-antiproton collisions together with its antiparticle. We assume that the t' quark is a narrow resonance and always decays to Wq . We select lepton+jets final states with one isolated electron or muon with high transverse momentum (p_T), missing transverse momentum, and at least four jets corresponding to events in which one of the W bosons decays to leptons and the other W boson decays to jets. A similar search has been carried out by CDF using 4.6 fb^{-1} of data and resulted in the exclusion of such t' quarks at the 95% CL for masses below 335 GeV [5].

II. THE D0 DETECTOR

The D0 detector consists of central tracking, calorimeter, and muon detection systems [6] [7]. The magnetic central-tracking system consists of a silicon microstrip tracker and a scintillating fiber tracker, both located inside a 2 T superconducting solenoidal magnet. Central and forward preshower detectors are located just outside of the coil and in front of the calorimeters. The liquid-argon/uranium calorimeter is divided into a central section covering pseudorapidity $|\eta| \leq 1.1$ and two end calorimeters extending coverage to $|\eta| \leq 4$. The calorimeter is longitudinally segmented into electromagnetic, fine hadronic, and coarse hadronic sections with increasingly coarser sampling. Scintillators between the calorimeter cryostats provide sampling of showers at $1.1 < |\eta| < 1.4$. The muon system is located outside the calorimeter and consists of a layer of tracking detectors and scintillation trigger counters before 1.8 T toroids, followed by two similar layers outside the toroids. The trigger and data acquisition systems are designed to accommodate the high luminosities of Run II. Based on information from tracking, calorimeter, and muon systems, the output of the first level of the trigger is used to limit the rate for accepted events to $\approx 1.5 \text{ kHz}$. At the next trigger stage, with more refined information, the rate is reduced further to $\approx 800 \text{ Hz}$. These first two levels of triggering rely mainly on hardware and firmware. The third and final level of the trigger, with access to all the event information, uses software algorithms and a computer farm, and reduces the output rate to $\approx 100 \text{ Hz}$, which is written to tape.

III. DATA SAMPLES AND MONTE CARLO SIMULATION

This analysis is based on data collected between June 2006 and September 2009 by the D0 Collaboration at the Fermilab Tevatron proton-antiproton collider at a center of mass energy of $\sqrt{s} = 1.96 \text{ TeV}$. The events must fire one of several trigger conditions, all requiring an isolated electron or muon with high transverse momentum (p_T), in some cases in conjunction with one or more jets. The integrated luminosity is 4.3 fb^{-1} .

For the $t'\bar{t}'$ signal generation we use PYTHIA [8] and set the branching fraction for the decay $t' \rightarrow Wb$ to 100%. Since we do not tag b -jets in the analysis our results are also applicable to heavy quarks decaying to a W boson and a light quark. We assume that the t' is a narrow resonance and set its total width to 10 GeV, independent of its mass. With this value the intrinsic width is much smaller than the resolution with which we can reconstruct the t' mass and the exact value does therefore not affect the analysis. We generated about 200,000 events for each of the 13 t' -mass values between 200 and 500 GeV.

Samples simulating $t\bar{t}$ production were generated with ALPGEN [9] at the matrix element level. Jets were filled in by parton showers generated by PYTHIA, followed by the detector simulation implemented using GEANT [10]. The top quark mass was set to 172.5 GeV and the factorization scale was set to $m_t^2 + \sum p_T^2(\text{jets})$. We normalize the $t\bar{t}$ sample to the expected $t\bar{t}$ production cross section of $7.48_{-0.72}^{+0.56}$ pb [11].

W +jets samples were generated using ALPGEN and PYTHIA with a jet-matching algorithm, following the MLM prescription [12]. Three subsamples were generated: $Wb\bar{b}$, $Wc\bar{c}$ plus extra light partons and W +light partons. The matching algorithm ensures that jets generated by ALPGEN at the parton level and jets filled in by PYTHIA do not populate the same region in phase space, thus avoiding double counting in certain regions of ΔR and p_T space for the radiated jets. The factorization scale was set to $m(W)^2 + p_T(W)^2$. We also remove events with heavy flavor jets added by PYTHIA to avoid duplicating the phase space of those already generated by ALPGEN. Wc subprocesses are included in the W +light parton sample with massless charm quarks. We increase the number of $Wb\bar{b}$ and $Wc\bar{c}$ events relative to W +light partons to match NLO cross sections.

$Z(\rightarrow ee, \mu\mu, \tau\tau)$ +jets, samples were generated with ALPGEN and PYTHIA and broken up into $Zb\bar{b}$, $Zc\bar{c}$, and $Zq\bar{q}/Zgg$ plus light parton samples in the same way as the W +jets samples. We normalize the Z samples to the NNLO cross section of 256 pb [13], 1.3 times the leading-order cross section given by ALPGEN, and increase the relative population of $Zb\bar{b}$ by a factor 1.52 and of $Zc\bar{c}$ by 1.67, respectively. We simulate single top quark production using the COMPHEP-SINGLETOP [14] Monte Carlo event generator with the top quark mass set to 172.5 GeV. The cross section for single top production computed to NNLO with NNNLO threshold corrections in the s and t -channels is 3.3 pb [15]. Diboson samples were generated with PYTHIA. Their NLO cross sections are 12.3 pb for WW , 3.7 pb for WZ , and 1.4 pb for ZZ -production [16].

For all Monte Carlo samples the CTEQ6L1 pdf set [17] was used.

IV. EVENT SELECTION

The final data sample is selected using the following criteria. For all events the $p\bar{p}$ collision point must be reconstructed with at least three tracks and located within 60 cm of the center of the detector. All events must have at least four jets with pseudorapidity $|\eta| < 2.5$ with respect to the center of the detector, $p_T > 40$ GeV for the leading jet and $p_T > 20$ GeV for all other jets.

Jets are reconstructed from energy deposits in the calorimeter using the Run II cone algorithm [18]. All jets must have at least two reconstructed tracks within the jet cone. The energy of jets is corrected so that it matches on average the total energy of all particles emitted inside the jet cone. Jets containing a muon within $R < 0.5$ of the jet axis are considered to originate from a semileptonic b -quark decay and are corrected for the momentum carried away by the muon and the neutrino. For this correction, it is assumed that the neutrino carries the same momentum as the muon. Jets in simulated events are adjusted to reproduce the jet reconstruction efficiency, the energy resolution, and the calorimeter response observed in the data.

The momentum carried away by neutrinos can be inferred using momentum conservation in the transverse plane. The sum of the transverse momenta of all neutrinos is equal to the negative sum of the transverse momenta of all particles that were observed in the detector. In practice we compute the missing transverse momentum \cancel{p}_T by adding up vectorially $E\hat{x}_T$ for all cells of the electromagnetic and fine hadronic calorimeters. Here E is the energy deposit in the cell and \hat{x}_T is a two-component vector consisting of the two transverse components of the unit vector that points from the collision point to the cell center. Cells in the coarse hadronic calorimeter are only added if they are part of a jet. This quantity is then corrected for the energy corrections applied to the reconstructed jets and leptons, and for the momentum of all muons in the event, taking into account their energy loss in the calorimeter.

Electrons are clusters of energy depositions in the electromagnetic section of the calorimeter consistent in shape with an electromagnetic shower. At least 90% of their energy must be in the electromagnetic section of the calorimeter and the energy deposition pattern must be consistent with an electromagnetic shower. Electron candidates must be sufficiently isolated from other energy depositions in the calorimeter so that the fraction of energy in an annular isolation cone of radius $0.2 < R < 0.4$, $R = \sqrt{\Delta\phi^2 + \Delta\eta^2}$ is less than 15% of the energy in the core cone of radius $R < 0.2$. Here ϕ is azimuth and η is pseudorapity. Every electron must be matched to a charged particle track from the tracking detectors with $p_T > 5$ GeV. Electrons must pass an additional cut on the combined likelihood of all electron identification variables.

For the e +jets channel we require one isolated electron with $p_T > 20$ GeV and $|\eta| < 1.1$ that originates from the $p\bar{p}$ collision point. No second isolated lepton with $p_T > 15$ GeV is allowed and we require $\cancel{p}_T > 20$ GeV and $\Delta\phi(e, \cancel{p}_T) > 2.2 - 0.045\cancel{p}_T$. In this channel we find a total of 1002 events.

Muons are reconstructed primarily as tracks in the muon spectrometer. We reject cosmic rays by requiring hits in the muon scintillation counters within 10 ns of the beam crossing time. The track reconstructed in the muon system must match a track reconstructed in the central tracker that originates from the beam line. Muons must be separated

from jets by $R > 0.5$. The energy deposited in an annular cone of radius $0.1 < R < 0.4$ around the muon direction must be less than 8% of the p_T of the muon and the momenta of all tracks in a cone of radius $R = 0.5$ around the muon direction, except the track matched to the muon, must add up to less than 6% of the p_T of the muon.

For the μ +jets channel we require one muon with $p_T > 20$ GeV and $|\eta| < 2$ that originates from the $p\bar{p}$ collision point. No second isolated lepton with $p_T > 15$ GeV is allowed. The invariant mass of the selected muon and any second muon must be less than 70 GeV or more than 110 GeV to reject $Z(\rightarrow \mu\mu)$ +jet events. We require $\cancel{p}_T > 25$ GeV and $\Delta\phi(\mu, \cancel{p}_T) > 2.1 - 0.035 \cdot \cancel{p}_T$. In this channel we find a total of 807 events.

The cuts on the azimuthal separation between lepton and missing p_T reject events in which energy depositions were misidentified as leptons. Since their energy is likely to be mismeasured they give rise to an imbalance in the transverse momentum along the direction of the lepton. The total efficiency of the event selection for the t' -signal samples is listed in Table III.

V. BACKGROUND MODEL

The main two standard model processes that produce events with an isolated lepton, missing p_T , and at least four jets are $t\bar{t}$ production and W +jets production. Single top, Z +jets, and diboson production can also give rise to such a final state but have much smaller cross sections. The third most important source of events arises from multijet events in which energy depositions from a jet are misidentified as a lepton and missing p_T is mismeasured.

In order to build our background model we first estimate the number of multijet events that enter the final data sample using measured selection efficiencies and a loose data sample that is a superset of the final data sample for this analysis and was selected using less stringent cuts for the identification of the leptons. The number of events in the loose and final data samples are denoted by N' and N , respectively. $N^{\ell j}$ denotes the combined number of events with genuine leptons in the loose sample, N^{jj} corresponds to the number of multijet events in the loose sample, ε_ℓ is the efficiency for a lepton in the loose sample to also pass the final lepton selection, and ε_j is the efficiency for a misidentified jet in the loose sample to also pass the final lepton selection. With these definitions, one can write the following equations:

$$N' = N^{\ell j} + N^{\text{jj}} \quad \text{and} \quad N = \varepsilon_\ell N^{\ell j} + \varepsilon_j N^{\text{jj}} \quad (1)$$

Solving this system of equations for N^{jj} and $N^{\ell j}$ yields:

$$N^{\ell j} = \frac{N - \varepsilon_j N'}{\varepsilon_\ell - \varepsilon_j} \quad \text{and} \quad N^{\text{jj}} = \frac{\varepsilon_\ell N' - N}{\varepsilon_\ell - \varepsilon_j}. \quad (2)$$

The efficiency ε_ℓ for true leptons is $86.9 \pm 2.2\%$ for e +jets events and $93.9 \pm 2.2\%$ for μ +jets events as obtained from the corresponding W +jets and $t\bar{t}$ Monte Carlo samples. The efficiency ε_j for fake leptons to pass the tight isolation selection is measured directly from data. We use events with $\cancel{p}_T < 10$ GeV which are dominated by misidentified leptons to calculate ε_j as the ratio of number of events in the final and in the loose data samples. For e +jets events $\varepsilon_j = 13.0 \pm 3.0\%$ and for μ +jets events $\varepsilon_j = 30.6 \pm 3.1\%$.

In this way we compute the number of multijet events in the e +jets and μ +jets samples separately. We then subtract the multijet background and all other backgrounds based on their calculated cross sections except the W +jets background from the data and equate the W +jets contribution to the remaining number of events. Table I summarizes the resulting composition of the final data sample.

TABLE I: Composition of the final data sample. Here the number of W +jets events was chosen to equalize the total number of events observed and expected.

source	number of e +jets events	number of μ +jets events
$t\bar{t}$ production	573	401
single t production	10	7
W +jets	255	338
Z +jets	29	28
WW, WZ, ZZ +jets	20	16
multijets	115	16
data	1002	807

VI. ANALYSIS

We use two variables to distinguish the t' -signal from the standard model backgrounds, the reconstructed t' -mass and H_T , the scalar sum of the transverse momenta of all jets, the charged lepton, and the missing p_T in the event. Both exploit the large mass of the t' quark. We reconstruct the mass of the t' quark using a kinematic fit to the $t't' \rightarrow \ell\nu b\bar{q}\bar{q}'\bar{b}$ hypothesis. The χ^2 of the kinematic fit is given by

$$\chi^2 = \sum_{i=\ell, j_1 \dots j_4} \left\{ \left(\frac{p^i - p_{fit}^i}{\delta p^i} \right)^2 + \left(\frac{\phi^i - \phi_{fit}^i}{\delta \phi^i} \right)^2 + \left(\frac{\eta^i - \eta_{fit}^i}{\delta \eta^i} \right)^2 \right\} + \left(\frac{k^x - k_{fit}^x}{\delta k^x} \right)^2 + \left(\frac{k^y - k_{fit}^y}{\delta k^y} \right)^2, \quad (3)$$

where the sum runs over the charged lepton and the four leading jets and

$$\vec{k}_T = \begin{pmatrix} k^x \\ k^y \end{pmatrix} = \vec{p}_T + \sum_{i=\ell, j_1 \dots j_4} p_T^i. \quad (4)$$

This χ^2 is minimized subject to the constraints $m(\ell, \nu) = m(j_3, j_4) = m_W$ and $m(\ell, \nu, j_1) = m(j_2, j_3, j_4) = m_{fit}$. Both solutions for $p_z(\nu)$ that satisfy the constraint $m(\ell, \nu) = m_W$ are considered. We consider all possible assignments of the leading four jets $j_1 \dots j_4$ to the four quarks in the final state. The kinematic fit converges for the t' with an efficiency of 100% in the e +jets channel and 98%-100% in the μ +jets channel. In choosing the best permutation we add another term to the χ^2 from Equation 3

$$\Delta\chi^2 = (((p_T(\ell, \nu, j_1) + p_T(j_2, j_3, j_4))/2 - 90 \text{ GeV}) / 60 \text{ GeV})^2 \quad (5)$$

where 90 GeV is the mean and 60 GeV the rms of the p_T distribution of a massive t' quark. We choose the value for the free parameter m_{fit} that minimizes $\chi^2 + \Delta\chi^2$. We observe that the two permutations that differ by exchange of the jets assigned to the two b quarks often have similar values of χ^2 but the permutation with the lower t' p_T is more often the correct assignment. The additional term prefers permutations with lower t' p_T values and thus helps in selecting the correct permutation. Figures 1 and 2 show the expected distributions of H_T and m_{fit} from data and from the expected standard model backgrounds. The expected signal from a 300 GeV t' quark is superimposed.

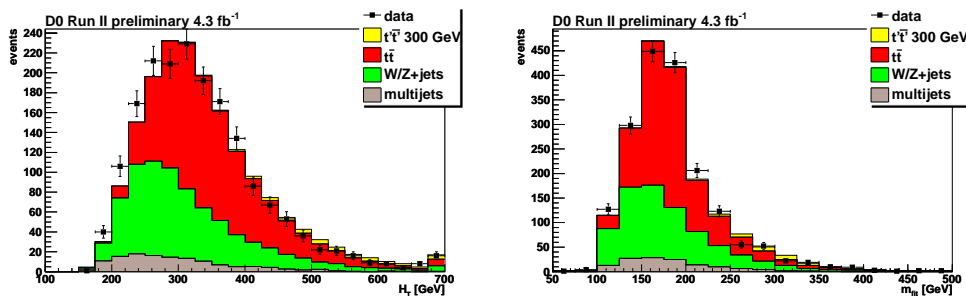


FIG. 1: Distributions of H_T and m_{fit} for data compared with expectations. The W/Z +jets category also includes Z +jets, single top quark, and diboson production. The $t't'$ signal is normalized to the expected yield. The number of W/Z +jets events was reduced accordingly relative to the values in Table I to make the integral of the model equal to the number of events in the data sample.

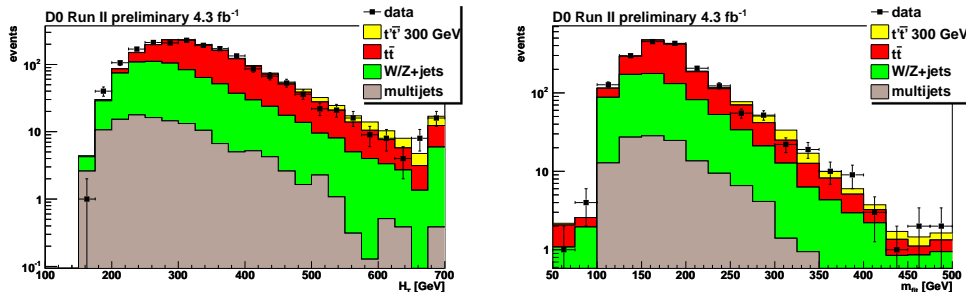


FIG. 2: Same as Fig. 1 except with logarithmic scale for the y -axis.

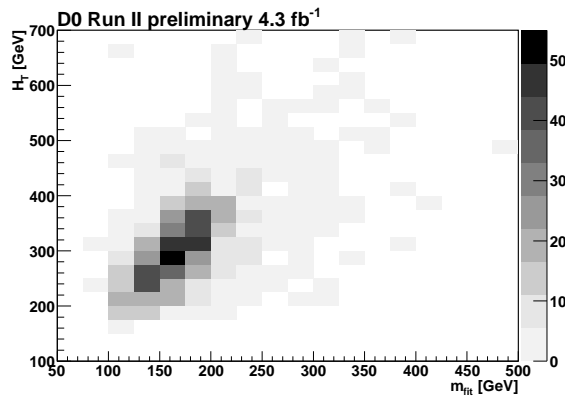


FIG. 3: Two-dimensional histogram of H_T versus m_{fit} for the final data sample.

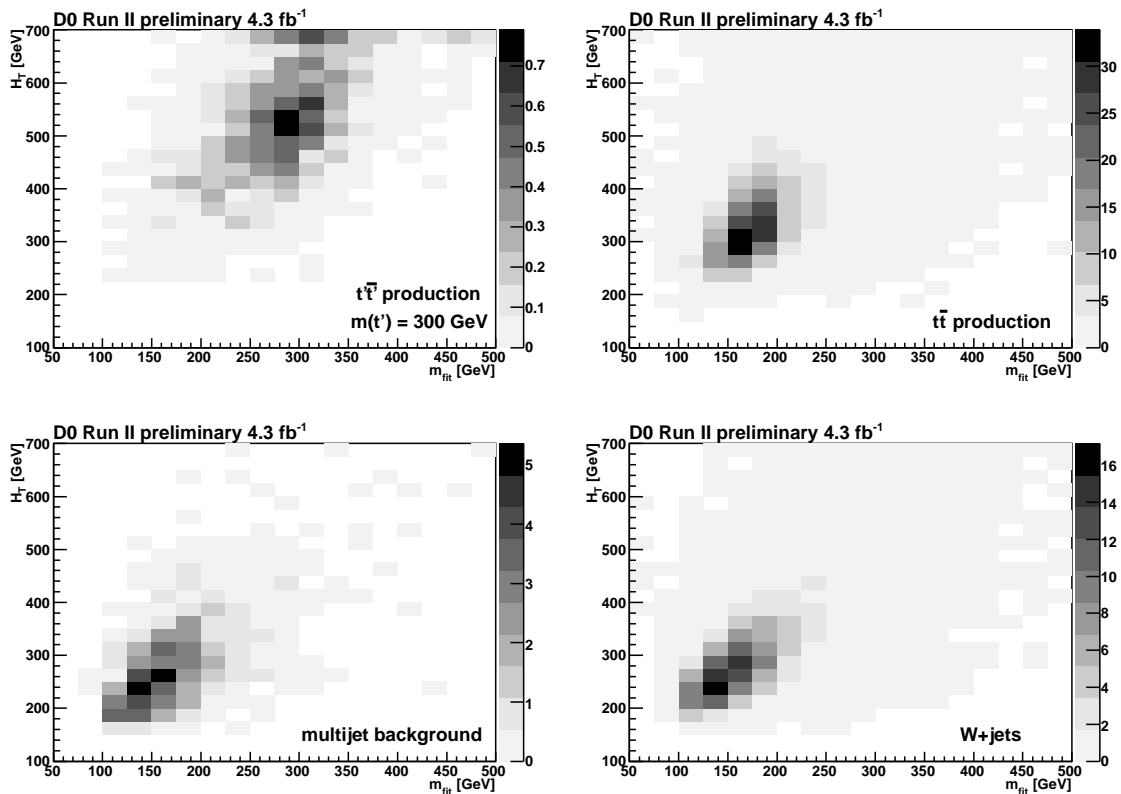


FIG. 4: Two-dimensional histograms of H_T versus m_{fit} for 300 GeV t' -signal, $t\bar{t}$ -production, multijet backgrounds, and W +jets and all other backgrounds.

We use the two-dimensional histograms of H_T versus m_{fit} to test for the presence of a signal from $t'\bar{t}'$ production in the data and compute 95% CL upper limits on the $t'\bar{t}'$ production cross section as a function of t' -mass. Figure 3 shows the observed distribution. For each hypothesized value of the t' mass, we fit the data assuming a background only hypothesis and assuming a signal plus background hypothesis. We then use as test statistic the likelihood ratio

$$L = -2\log\frac{P_{S+B}}{P_B}, \quad (6)$$

where P_{S+B} is the Poisson likelihood to observe the data under the signal plus background hypothesis and P_B is the Poisson likelihood to observe the data under the background only hypothesis. For the background only hypothesis three components are fit to the data: $t\bar{t}$ production constrained to its cross section of 7.48 pb, the multijets background

constrained to the number of events given in Table I with an uncertainty given in Table II, and W +jets and all other backgrounds in the proportions given in Table I with an overall normalization that floats freely. For the signal plus background fit we also include the $t'\bar{t}$ signal which floats freely. We can float background and signal contributions because the shapes of their H_T and m_{fit} distributions are very different as shown in Fig. 4. For each hypothesis we vary all the systematics given in Table II to maximize a profile likelihood function [20].

To determine the cross section limits we use the CL_s method [19]. Using pseudoexperiments, we determine the probability to measure values of L that are larger than the value observed in our data sample assuming that there is a t' -signal, CL_{s+b} , and assuming that there is no t' -signal, CL_b . The value of the t' -pair production cross section for which $1 - CL_{s+b}/CL_b = 0.95$ is the 95% CL upper limit. We repeat this procedure for every t' -mass point.

Table II summarizes the sources of systematic uncertainties included in the calculation. The top four uncertainties in the Table affect the normalization of the components of our signal and background models. All other uncertainties affect the preselection efficiency. We also consider uncertainties in the shape of the H_T and m_{fit} distributions that arise from uncertainties in the jet energy scale calibration, the jet identification efficiency and the jet energy resolution. To evaluate these uncertainties we allow the shape of the H_T and m_{fit} distributions to vary in the limit calculation.

TABLE II: Summary of systematic uncertainties

source	e+jets channel			μ +jets channel		
	$t'\bar{t}$	$t\bar{t}$	multijets	$t'\bar{t}$	$t\bar{t}$	multijets
$t\bar{t}$ cross section	-	+8%/-10%	-	-	+8%/-10%	-
multijets normalization	-	-	$\pm 4.7\%$	-	-	$\pm 52\%$
branching fractions	$\pm 0.8\%$	$\pm 0.8\%$	-	$\pm 0.8\%$	$\pm 0.8\%$	-
integrated luminosity	$\pm 6.1\%$	$\pm 6.1\%$	-	$\pm 6.1\%$	$\pm 6.1\%$	-
initial and final state radiation	+0.5%/-3.7%	+4.4%/-0.7%	-	+0.8%/-2.4%	+1.1%/-3.9%	-
MC model	-	$\pm 4.3\%$	-	-	$\pm 4.3\%$	-
parton distribution functions	+0.7%/-1.1%	+0.22%/-0.42%	-	+0.7%/-1.1%	+0.14%/-0.25%	-
trigger efficiency	+0.3%/-1.7%	+0.4%/-1%	-	0	0	-
primary vertex id	$\pm 1.6\%$	$\pm 1.6\%$	-	$\pm 1.6\%$	$\pm 1.6\%$	-
jet energy calibration	shape	shape	-	shape	shape	-
jet energy resolution	shape	shape	-	shape	shape	-
jet identification	shape	shape	-	shape	shape	-
electron identification	$\pm 3.8\%$	$\pm 3.8\%$	-	-	-	-
muon identification	-	-	-	$\pm 2.9\%$	$\pm 2.9\%$	-

Figure 5 shows the resulting cross section limits as a function of t' -mass, compared to the limit expected in the absence of t' -production and to the predicted t' -pair production cross section. The results are also tabulated in Table III.

TABLE III: Summary of t' -pair production cross section, selection efficiency, expected number of events, and 95% CL upper limits on the cross section.

t' -mass	theory cross section (pb)	t' events	t' efficiency	expected limit (pb)	observed limit (pb)
200 GeV	3.189	441.	19%	0.84	1.6
225 GeV	1.400	218.	21%	0.52	0.62
250 GeV	0.800	133.	23%	0.30	0.43
275 GeV	0.430	75.	24%	0.22	0.33
300 GeV	0.227	44.	27%	0.14	0.24
325 GeV	0.121	23.5	27%	0.11	0.23
350 GeV	0.064	12.6	27%	0.085	0.17
375 GeV	0.034	7.0	28%	0.068	0.15
400 GeV	0.018	3.7	27%	0.058	0.12
425 GeV	0.010	2.0	27%	0.050	0.10
450 GeV	0.005	1.0	27%	0.045	0.078
475 GeV	0.003	0.5	26%	0.042	0.063
500 GeV	0.001	0.3	25%	0.041	0.064

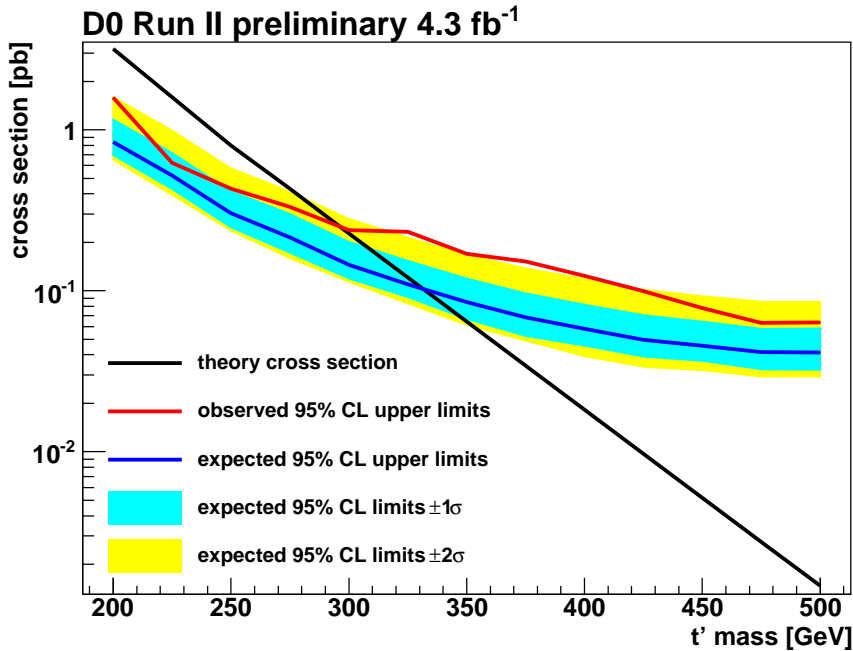


FIG. 5: Observed and expected upper limits and predicted values for the $t'\bar{t}'$ production cross section as a function of the mass of the t' quark. The dotted lines indicate the limits obtained without systematic uncertainties

VII. CONCLUSION

We have searched for pair production of a t' quark and its antiparticle followed by their decays into Wq using 4.3 fb^{-1} of data collected by the D0 Collaboration at the Fermilab Tevatron collider. We set 95% CL upper limits on the production cross section for such t' quarks. By comparing with the predicted production cross section we can exclude pair production of t' quarks with masses below 296 GeV at 95% CL. The expected limit for our search based on MC simulations is 330 GeV.

Acknowledgements

We thank the staffs at Fermilab and collaborating institutions, and acknowledge support from the DOE and NSF (USA); CEA and CNRS/IN2P3 (France); FASI, Rosatom and RFBR (Russia); CNPq, FAPERJ, FAPESP and FUNDUNESP (Brazil); DAE and DST (India); Colciencias (Colombia); CONACyT (Mexico); KRF and KOSEF (Korea); CONICET and UBACyT (Argentina); FOM (The Netherlands); STFC and the Royal Society (United Kingdom); MSMT and GACR (Czech Republic); CRC Program and NSERC (Canada); BMBF and DFG (Germany); SFI (Ireland); The Swedish Research Council (Sweden); and CAS and CNSF (China).

-
- [1] C. Amsler et al. (Particle Data Group), Phys. Letters B **667**, 1 (2008).
 - [2] V.A. Nobikov et al., arXiv:hep-ph/0111028v3, January 2002.
 - [3] P.H. Frampton et al., Physics Reports **330**, 263 (2000).
 - [4] T. Han et al., Physical Review D **67**, 095004 (2003).
 - [5] CDF Collaboration, “Search for heavy top $t' \rightarrow Wq$ in lepton plus jets events in $\int \mathcal{L} dt = 4.6 \text{ fb}^{-1}$ ”, CDF note 10110, March 2010.
 - [6] D0 Collaboration, S. Abachi *et al.*, Nucl. Instrum. Methods Phys. Res. A **338**, 185 (1994).
 - [7] D0 Collaboration, V.M. Abazov *et al.*, Nucl. Instrum. Methods Phys. Res. A **565**, 463 (2006).
 - [8] T. Sjöstrand, S. Mrenna, and P. Skands, JHEP 0605:026 (2006) (version 6.409).
 - [9] M. L. Mangano *et al.*, J. High Energy Phys. **07**, 001 (2003) (version 2.11).
 - [10] R. Brun and F. Carminati, CERN Program Library Long Writeup W5013, 1993 (unpublished).

- [11] Moch and Uwer, Physical Review D **78**, 034003 (2008).
- [12] S. Höche *et al.*, “Matching Parton Showers and Matrix Elements”, hep-ph/0602031.
- [13] R. Hamberg, W.L. van Neerven and W.B. Kilgore, Nucl. Phys. B **359**, 343 (1991) and erratum in B **644**, 403 (2002). The cross section was corrected to include the γ^* contribution.
- [14] E.E. Boos *et al.*, Phys. Atom. Nucl. **69**, 1317 (2006).
- [15] N. Kidonakis, Phys. Rev. D **74**, 114012 (2006).
- [16] computed with MCFM: J. Campbell and R.K. Ellis, MCFM - Monte Carlo for FeMtobarn processes, <http://mcfm.fnal.gov/>.
- [17] J. Pumplin *et al.*, J. High Energy Phys. **07**, 012 (2002) and D. Stump *et al.*, J. High Energy Phys. **10**, 046 (2003).
- [18] G. Blazey *et al.*, in *Proceedings of the Workshop: “QCD and Weak Boson Physics in Run II”* edited by U. Baur, R.K. Ellis and D. Zeppenfeld, FERMILAB-Pub-00/297 (2000).
- [19] T. Junk, Nucl. Instrum. Methods Phys. Res., A **434**, 435 (1999).
- [20] W. Fisher, FERMILAB-TM-2386-E.